AIAA JOURNAL
Vol. 38, No. 4, April 2000

Wake of a Self-Propelled Body, Part 2: Momentumless Wake with Swirl

A. I. Sirviente*
University of Michigan, Ann Arbor, Michigan 48109-2145
and
V. C. Patel†
University of Iowa, Iowa City, Iowa 52242-1585

Experiments were performed in the near wake of an axisymmetric body propelled by a swirling jet. Comparisons with parallel experiments in the drag wake of the bare body without the jet and in the isolated swirling jet provide insights on the mixing between the component flows and their evolution into the momentumless wake with swirl. Comparisons with the momentumless wake without swirl analyze the effect of swirl in this type of wake. Comparison with experimental data in the wake of the same body propelled by a marine propeller are also presented. Hot-wire and pressure probes were used in a wind tunnel to measure the mean velocity, turbulence, and pressure fields from the jet exit to a distance of over 15 jet diameters. The wake evolves in at least three distinct stages: a zone close to the jet exit where the jet periphery mixes with the wall region of the body boundary layer, an intermediate region where the mixing between the boundary layer and the jet spreads up to the axis, and a region where the two flows lose their identities to become a single shear layer in which there is negligible turbulence production.

I. Introduction

THE wake of an axisymmetric body fixed in a wind tunnel is characterized by a deficit of axial momentum equal to the drag on the body. On the other hand, there are three types of momentumless axisymmetric wakes, and all are relatively unknown members of canonical turbulent shear flows that admit similarity solutions sufficiently far from their origins. Momentumless wakes are generated by self-propelled bodies, the most common forms of propulsion being a jet or a propeller. The three classes depend on whether the flow is without or with swirl. Only a simple jet can provide streamwise momentum without swirl; this constitutes the first class. The other two classes depend on the amount of the axial flux of tangential momentum present. If swirl is provided by a propeller or a swirling jet to a fixed body, as might be the case in a body fixed in a wind tunnel, then the axial flux of tangential momentum is equal to the torque required to restrain the body. On the other hand, the wake of an unrestrained self-propelled body, driven by two matched counter-rotating propellers, has no net flux of either axial or tangential momentum, although it has swirl. In two previous papers the authors have described experiments on the drag wake[1] and the momentumless wake without swirl.[2] The present study is concerned with a momentumless wake with a nonzero tangential momentum flux. For this case, the axisymmetric body of the previous experiments was propelled by a swirling jet issuing from its base.

To the authors' knowledge, only momentumless swirling wakes generated by propeller-driven bodies have been investigated in the past. While adding momentum and swirl, a propeller adds unsteadiness, three dimensionality and high levels of turbulence to the turbulent shear flow coming from the body boundary layer. Even in the case of an axisymmetric body with a coaxial propeller, the flow behind the propeller is three dimensional due to the individual blade wakes. The flow is rotationally symmetric only in a circumferentially averaged sense. For example, a quite detailed investigation of the wake of a body driven by a three-blade propeller was conducted by Hyun and Patel[3,4] and more recently by Faure and Robert.[5] The present study is related to the former insofar as the same body shape is employed and the main effects of the propeller, namely, the addition of axial and circumferential momenta, are reproduced here by means of a swirling jet issuing from the tail of the body. This paper presents and discusses the experimental data corresponding to the momentumless wake of a swirling, jet-propelled axisymmetric body. The effect of swirl is discussed, and comparisons are presented between a momentumless wake with and without swirl.[2] The (self-propelled) data of Hyun and Patel[3,4] are also compared with the present data.

II. Design of Experiments

The axisymmetric body described by Sirviente and Patel[1,2] was also used for this study (Figs. 1a and 1b). The body has a length L of 143.45 cm, a maximum radius R of 6.95 cm and a base diameter of 3.96 cm, allowing a coaxial jet of diameter $D = 3.90$ cm to be introduced from the tail. The boundary layer on the body was tripped by a 1.2-mm-diam wire located 9.5 cm from the nose. Air was supplied through a 1.24-cm-diam pipe along the body axis entering the body at the nose to provide axial momentum to the jet exiting at the tail. To impart tangential momentum to the jet, air was also introduced through a 3-cm-diam concentric pipe surrounding the first pipe (Fig. 1b). The tangential flow was injected 39 cm upstream from the jet exit through four 1.0×0.5 cm tangential slots. This method of swirl generation based on the combination of an axial and a tangential flow is simple, has no moving parts, and provides independent control of the axial and tangential momentum introduced in the flow.

The experiments were conducted in a 1.07-m octagonal open test-section, return-circuit wind tunnel. Figure 1a shows the tunnel and model arrangement along with the coordinate system used to report the data. The freestream velocity U_o was set at 16.5 m/s, resulting in a Reynolds number based on the body length of 1.58×10^6. The jet was adjusted[2] such that its axial momentum was just enough to cancel the body drag. This condition resulted in a maximum axial velocity of $2U_o\,(=U_{sj})$ at 3 mm from the exit, giving a jet Reynolds number ($Re_{sj} = U_{sj}D/\nu$) of 8.6×10^4. The jet swirl was adjusted to match the torque of the propeller employed by Hyun and Patel.[3,4] This was achieved with a maximum swirl velocity at exit, $W_{sj} = 0.95U_o$.

Measurements in the axial direction extended to $x/D = 19.53$, where x is the distance from the body base, and in the radial direction to $r/R = 4.5$ to ensure recovery of freestream conditions. The measurements were made with a triple-sensor hot-wire probe along

Received 11 May 1998; revision received 26 July 1999; accepted for publication 29 August 1999.

*Assistant Professor, Department of Naval Architecture and Marine Engineering. Member AIAA.

†Professor, Department of Mechanical Engineering, and Director, Iowa Institute of Hydraulic Research. Associate Fellow AIAA.

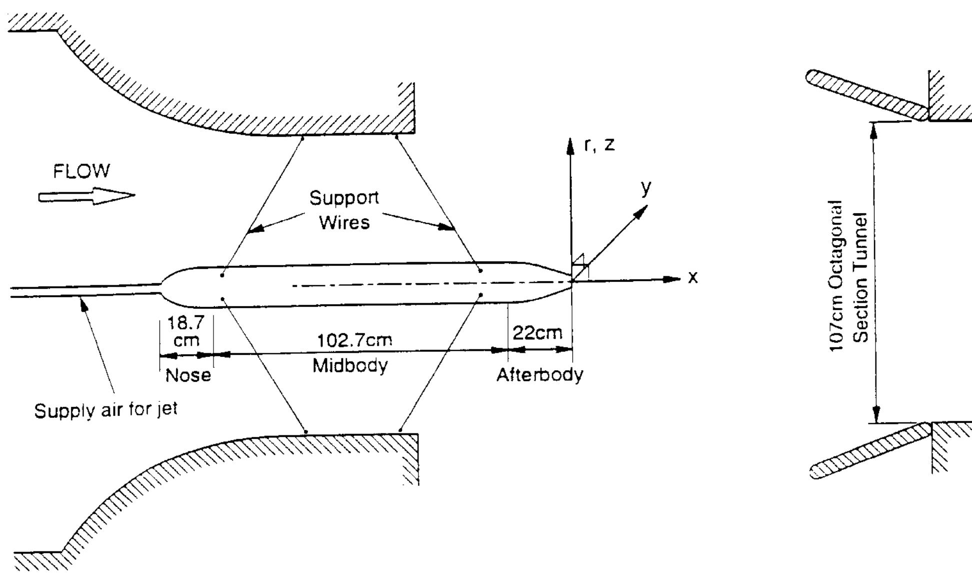

a) General arrangement

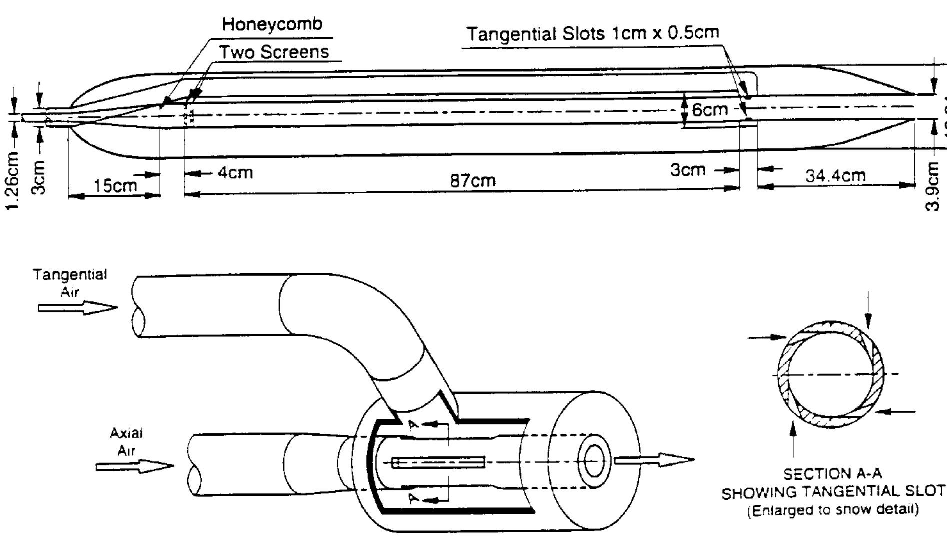

b) Modified Iowa body

Fig. 1 Wind tunnel and model arrangement.

with a five-hole pitot probe. A detailed description of the experimental equipment, instrumentation, and measurement procedures can be found in Ref. 6 (see also Ref. 2), along with an analysis of the uncertainty in the data [2% for (U, V, W), 10% for $\overline{uu}$ and $\overline{uv}$, and 20% for the rest of the Reynolds stresses].

III. Measurements in Component Flows

Measurements in the boundary layer over the body and in the near wake were previously described by Sirviente and Patel.[1] Therefore, in this section it will be sufficient to indicate that at $x/L = -0.180$ the usual boundary-layer parameters were momentum-thickness Reynolds number $R_\theta = U_o\theta/\nu = 845$, shape parameter $H = 1.29$, and friction coefficient $C_f = 0.0045$. The region of reverse flow extended up to $x/D = 0.551$.

Measurements were also made in the swirling jet issuing from the tail of the body without any ambient flow. The conditions of the swirling jet were discussed in Sec. II. The swirl number was $S = 0.34$, where S represents the ratio of tangential to axial momentum at exit:

$$S = \frac{M_{\theta x}}{M_x(R_j/D)} \tag{1}$$

where R_j is the nozzle or jet radius, $M_{\theta x}$ is the axial flux of tangential momentum, and M_x is the axial flux of axial momentum.

Because of the centrifugal forces present, the jet axial velocity maximum did not occur at the centerline until about 3–4 jet diameters. The distribution of the velocity scales showed no evidence of a jet core because both maximum and centerline velocities decayed continuously from the jet exit, whereas the half-radius, defined in the conventional way as the radius where the velocity is half of the centerline velocity, increased continuously. The present data showed an angle of spread of 11 deg and the virtual origin of the jet was extrapolated to be at $x_o/D = -3.31$. Further discussion related to the isolated swirling jet can be found by Sirviente.[6]

IV. Momentumless Wake with Swirl

A. Mean Flow

Figure 2 shows typical profiles of the axial U and tangential or swirl W components of mean velocity. It is clear that the axial flow is characterized by three velocities, namely, centerline U_c, minimum U_{mn}, and edge U_e, and at least three radii, b_1, where the local velocity is $(U_c - U_{mn})/2$; b_{mn}, where it is U_{mn}; and b_2, where it is $(U_e - U_{mn})/2$. In the near wake, yet another velocity scale, the maximum velocity U_m, different from U_c (not shown in Fig. 2) can be distinguished. The maximum swirl velocity W_m and the radius where it occurs b_{W_m} describe the tangential flow.

Figures 3 and 4 show the mean axial U and swirl W velocity profiles, respectively, at the six streamwise stations named A–F. A very rapid mixing between the boundary layer and the jet in the axial

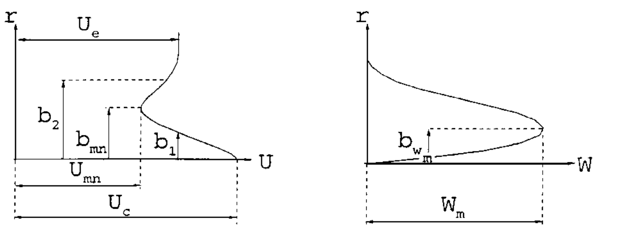

Fig. 2 Typical axial *U* and tangential *W* velocity profiles in a momentumless swirling wake.

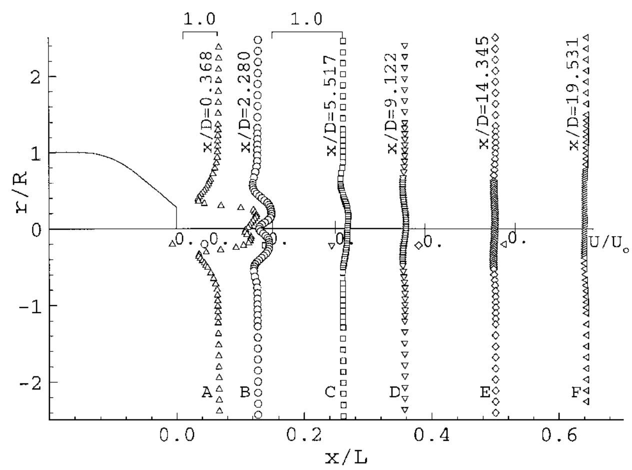

Fig. 3 Overview of flow in the momentumless swirling wake.

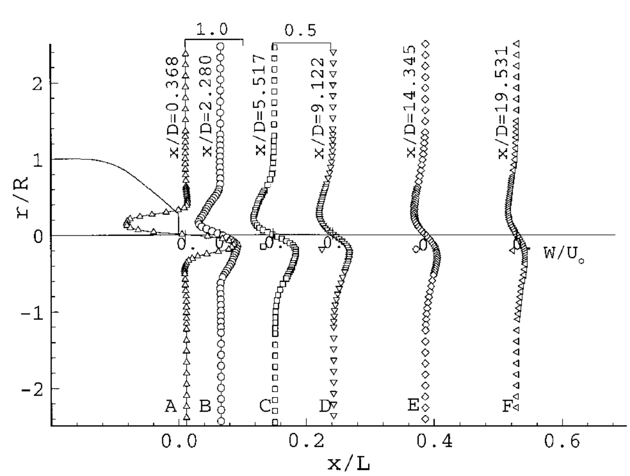

Fig. 4 Tangential velocity.

velocity is seen from these profiles, as well as a somewhat slower decay of swirl. The axial velocity profile shows a peculiar hump in the central part of the wake, with a maximum velocity larger than the centerline velocity. This is characteristic of jets with moderate to strong swirl. By $x/D = 4$, and well before station C, the velocity maximum occurs at the centerline and the profile is as shown in Fig. 2.

Figure 5 presents the evolution of the momentumless swirling wake velocity and length scales along with the prediction from similarity analysis (explained later in this section). Figure 5a shows that within a distance of about $x/D = 4$, the axial centerline velocity decreases from $2U_o$ at the jet exit to very close to $1.1U_o$, where it becomes coincident with the maximum velocity (not shown), and the minimum velocity increases from zero at the jet exit to $0.9U_o$. Thus, the usual small-defect assumption made in classical similarity theory of wakes is met quite early in this flow. However, Fig. 5b shows that it takes a distance of almost $15D$ for the maximum swirl velocity to decay from its value of $0.95U_o$ at the jet exit to $0.1U_o$.

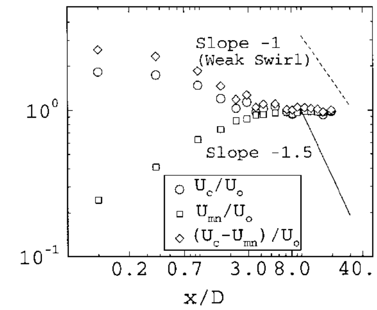

a) Axial velocity scales

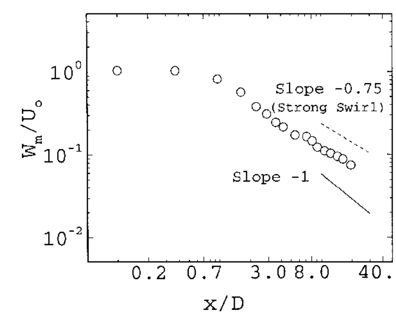

b) Tangential velocity scales

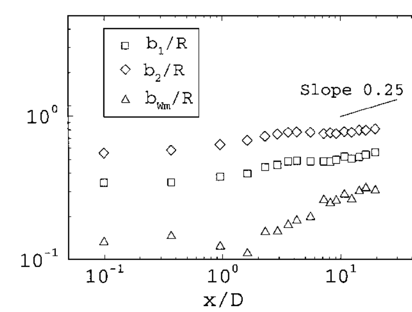

c) Length scales

Fig. 5 Wake velocity and length scales: - - - -, Ferry and Piquet,[7] and ——, Sirviente.[6]

Figure 5c shows that following an initial increase and a decrease, the length scale b_2, where the axial velocity is $(U_e - U_{mn})/2$, slowly increases after a streamwise distance of about $x/D = 10$. The scale b_1 increases from $D/2$ at the jet exit and follows a trend similar to b_2. The scale b_{W_m}, where the swirl velocity is maximum, increases from about $D/4$ and follows a trend similar to b_1 while remaining smaller than b_1. In other words, the location of maximum swirl velocity is much closer to the centerline than the minimum axial velocity, indicating a rather remarkable coherence of the swirl and its slow diffusion in the radial direction. All of these length scales are difficult to determine precisely from the data as the flow progresses downstream because the velocity variations across the wake become quite small.

Comparisons were made[6] between the measured mean velocity profiles corresponding to the momentumless swirling wake and those of the component flows. These comparisons are not shown here due to space restrictions, but the main conclusions are highlighted. At station A, the axial velocity profile of the momentumless wake is similar to that of the jet in the inner region and so is the tangential velocity component. By station B a considerable narrowing of the jetlike inner region of the momentumless wake takes place compared with the isolated jet. Thus, the boundary layer outside the jet exerts a large confining effect on the swirling jet. As a result of this, there is an increase in the swirl velocity over that measured in the isolated swirling jet. By station D the variation of the axial velocity across the momentumless swirling wake is far smaller than that in the jet and the bare-body wake. The swirl velocity on the other hand is still very significant compared with that measured in the isolated jet. Thus, it is concluded that in the swirling-jet propelled

Table 1 Power laws for an axisymmetric momentumless wake with swirl

Reference	l	U	W	$\overline{uv}_m$	$\overline{uw}_m$	$\overline{vw}_m$	k_m	ε_m	$(\bar{u}^2-\bar{v}^2)_m$	$(\bar{w}^2-\bar{v}^2)_m$
Ferry and Piquet[7] (weak swirl)	0.20	−0.8	−0.60	−1.60	——	−1.4	−1.6	−2.6	——	——
Ferry and Piquet[7] (strong swirl)	0.25	−1.0	−0.75	−1.75[a]	——	−1.5	−1.5	−2.5	——	——
Sirviente[6]	0.25	−1.5	−1.00	−2.25	−2.25	−1.5	−1.5	−5.5	−1.5	−1.5

[a]Corrected.

wake, the swirl decays at a much slower rate than in the isolated swirling jet. At the last station F, the swirling momentumless wake is considerably narrower than the isolated swirling jet but larger than the bare-body drag wake. Further details can be found in Ref. 6.

The evolution of the mass flux (not included) shows a rapid decrease in the near wake due to entrainment of the inviscid fluid by the boundary layer and vanishes beyond $x/D = 7$. The sum of the three terms in the axial momentum equation (convection, turbulence and pressure) is nowhere greater than 0.01 (1% of $0.5\rho U_o^2 R^2$). This is also a measure of the accuracy with which the self-propelled condition was realized in the experiments. The contribution of pressure to the axial momentum is significant until about $x/D = 13$. The negative pressure contribution is associated with increasing pressure in the axial direction and is compensated by decreasing convection of momentum by the mean flow. The contribution from the turbulence term is also quite significant in the near field, reaching a peak around $x/D = 2.5$. The flux of tangential momentum remains constant at 0.028 ± 0.002 along the wake. This value corresponds to that introduced by the propeller in the experiments of Hyun and Patel.[3,4]

On the basis of the mean-flow results presented in Figs. 3–5, the wake of the jet-propelled body may be subdivided into at least three regions: 1) the near field, $x/D < 3$, in which there is a rapid decrease in axial and swirl velocities due to the intense shear and mixing between the fluid from the near-wall region of the body boundary layer and the outer layers of the jet; 2) an intermediate region, $3 < x/D < 13$, where the pressure induced by the swirl continues to affect the momentum balance and the mixing between the boundary layer and the jet gradually encompasses the entire flow; and 3) the developed wake, $x/D > 13$, where the mixing is complete, the pressure returns to its ambient value, and the flow acquires some of the characteristics of a single shear flow. Experience with the momentumless wake without swirl,[2] however, suggests that this is a simplified picture.

It is of interest to inquire at what downstream distance a momentumless swirling wake achieves similarity conditions, if at all, or, alternatively, whether the flow in the developed-wake region $x/D > 13$ satisfies the requirements of similarity theory. Ferry and Piquet[7] and Sirviente[6] made the similarity analysis of axisymmetric momentumless wakes with swirl. The predicted exponents in the power laws of the various quantities are shown in Table 1, where l and U are the length and velocity scales, respectively, and the subscript m denotes scales (maxima). The results of the two analyses differ because of differences in the turbulence models and approximations made therein.[2] Ferry and Piquet[7] employed a k–ε turbulence closure, whereas Sirviente[6] used a Reynolds-stress transport model along with the experimental observation of negligible energy production in the transport equations.

Figure 5 also shows the comparison of the experimental data with the similarity analysis results shown in Table 1. As in the nonswirling case[2] the individual axial velocity scales U_c and U_{mn} do not follow either the −1.5 (Ref. 6) or the −1 (Ref. 7) power law and instead approach the freestream velocity U_o early in the streamwise development. The corresponding length scales b_1 and b_2 also do not grow with the expected 0.25 power. They appear to grow at a much slower rate. The uncertainty in the determination of the length scales, especially b_1, associated with the rapid decay of the axial velocity, is evident from Fig. 5. In spite of this, the velocity and length scales of the tangential velocity show behaviors consistent with the trends derived from similarity analysis by approximately $10D$. The different rates of growth and decay of the axial and tangential flows are quite surprising and would suggest that the mixing between boundary layer and jet is incomplete.

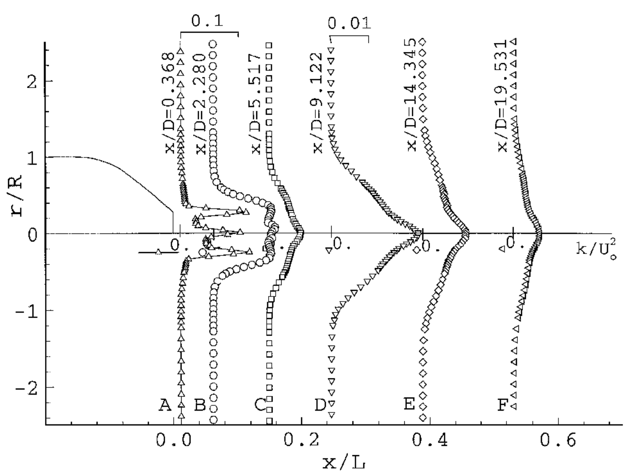

Fig. 6 Turbulence kinetic energy.

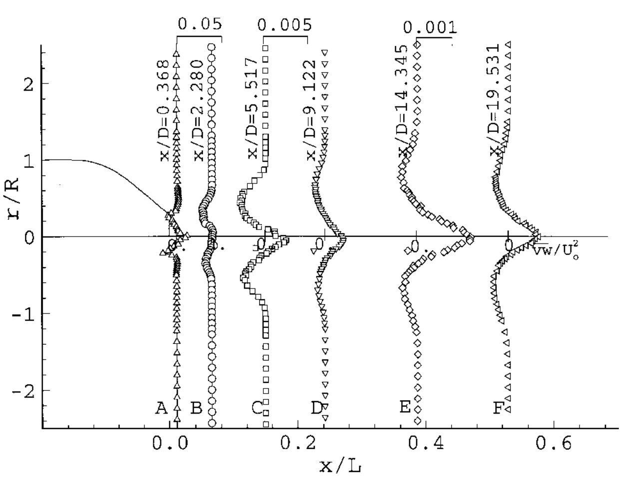

Fig. 7 Shear stress $\overline{vw}$.

B. Turbulence and Approach to Similarity

Although all six Reynolds stresses were measured, here consideration is restricted to the turbulence kinetic energy [defined as $k = \frac{1}{2}(\overline{uu} + \overline{vv} + \overline{ww})$] and two of the three shear stresses. The normal stresses at all stations are in the order: $\overline{ww} > \overline{vv} > \overline{uu}$, with the anisotropy persisting to the last station. Although none of the three shear stresses is zero in this flow, we shall consider only $\overline{uv}$ and $\overline{vw}$ because they comprise important terms in the axial and tangential momentum equations, respectively. Figures 6 and 7 show the evolution of the turbulence kinetic energy and $\overline{vw}$. The changes in scales in Figs. 6 and 7 were needed to accommodate the very large changes in these quantities as the flow evolves downstream.

The profiles in Figs. 6 and 7 show certain common features that are discussed first. At the first two stations (A and B), which lie in the previously defined near field, all turbulence profiles show the coexistence of two shear layers, one associated with the gradient of swirl velocity at the center and the other with the mixing zone between the jet and the boundary layer of the body (the boundary layer itself is not regarded as a separate shear layer). The centerline peaks in the turbulence quantities are associated with the swirl velocity, which is zero at the center and reaches a maximum before the interface between the jet and the body boundary layer. In fact, this peak is seen to persist at all downstream stations, another indication of the slower decay of swirl noted earlier (Fig. 5).

The turbulence profiles at the next two stations (C and D) indicate that mixing between the boundary layer and the jet gradually penetrates to the flow centerline. Recall that this was judged to be a feature of the intermediate wake. The magnitudes of the turbulence quantities have decreased such that an enlarged scale is needed to show the profile shape. It is significant that the shear stresses have practically vanished, being smaller than the estimated uncertainty limits of the data, although there remains significant levels of turbulent kinetic energy.

At the last two stations (E and F), lying in what was termed the developed-wake region on the basis of the mean flow, the magnitudes have further decreased such that yet another scale change is needed. Now the shapes of the shear-stress profiles have changed, but the data themselves are no longer meaningful in the light of their uncertainties. For all practical purposes, the shear stresses transporting axial (not shown) and tangential momentum have now vanished, and the turbulent kinetic energy slowly decays. It was found by Ridjanovic[8] and Wang[9] that a momentumless wake becomes shear free at a certain distance, where it could be considered as that produced by a point source of turbulence. The flow at the last two stations could be considered nearly homogeneous but anisotropic with almost uniform mean velocity. The intensity and length scales of k, $\overline{uv}$ and $\overline{vw}$, are plotted in Fig. 8 (where the subscript m denotes maxima), along with the power laws derived from similarity theory by Sirviente[6] (Table 1). As the maximum values of k and $\overline{vw}$ occur at the centerline, their length scales are taken as the radii, where the value is one-half of the maximum. The rapid decay of the shear stresses makes the determination of their length scales unreliable, especially in the last region of the development of the wake (Fig. 8). Figure 8a shows the three stages in the decay of k. The maximum value of k occurs at the wake centerline after the initial region (see Fig. 6). Similarly, Fig. 8b shows the vanishing of the $\overline{uv}$ shear stress within the intermediate zone, whereas Fig. 8c shows a slower collapse of the $\overline{vw}$ shear stress, as expected from the slower decay of swirl. Figure 8d shows the evolution of the turbulence length scales. They show a mixed behavior with only the length scale of the $\overline{vw}$ shear stress indicating the $\frac{1}{4}$ power growth predicted, whereas the scale of k shows a behavior closer to that expected for weak swirl, and that of $\overline{uv}$ shows a decay. The last feature is not entirely due to the low levels of stress and deterioration in the accuracy of the data, however; it is an indication that this is not yet a single shear layer, that is, the wake turbulence is not fully developed.

Comparisons of the turbulence profiles measured at the same locations in the bare-body wake, the isolated swirling jet and their combination, that is, the momentumless swirling wake were made.[6] In what follows the main conclusions are outlined. By station A all of the turbulence profiles show features that indicate superposition of the two component flows. At station D, on the other hand, all of the measurements indicate that the shear layers at the wake core and at the interface of the jet and the boundary layer have mixed across the flow. The multiple peaks in the turbulence profiles have disappeared by then. By the last station, F, the shear stresses $\overline{uv}$ and $\overline{uw}$ are of the order of $0.0004U_o^2$, much lower than those in the drag wake and the isolated jet and within the uncertainty limits of the data.

The velocity and tangential normal-stress profiles are plotted in Fig. 9 in the usual similarity format. For the axial velocity, two plots are made, normalizing $(U - U_{mn})$ and $(U - U_o)$ by $(U_c - U_{mn})$ and $(U_{mn} - U_o)$, to study the profiles in the inner and outer regions. The tangential velocity is normalized by its maximum value W_m, whereas $\overline{uu}_m$ is used for the turbulence quantities. The radial coordinate is normalized by the single length scale $b_{\overline{uu}_m/2}$, throughout.

The axial velocity profiles show that the inner and outer regions of the wake are governed by different scales, $(U_c - U_{mn})$ and $(U_{mn} - U_o)$, respectively. The data indicate that the inner and outer regions are matched at $r = b_{\overline{uu}_m/2}$. These results are similar to those of the non-swirling case,[2] and suggest an incomplete mixing of the inner and outer flows. The tangential velocity, on the other hand, seems to show similarity, confirming the results shown in Fig. 5b.

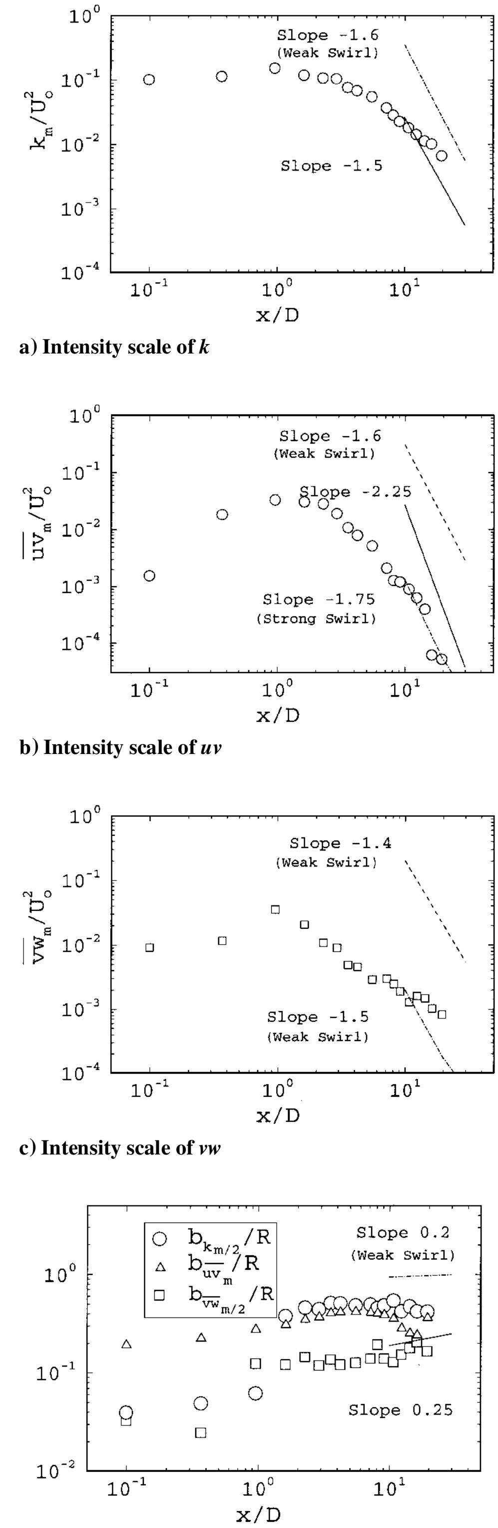

a) Intensity scale of k

b) Intensity scale of uv

c) Intensity scale of vw

d) Turbulence length scales

Fig. 8 Momentumless wake turbulence characteristics: - - - -, Ferry and Piquet,[7] and ——, Sirviente.[6]

The profiles of axial (not shown) and tangential normal stresses show similarity of shape, particularly in the inner region. This could be attributed to a length scale representative of the inner region being used.

V. Effect of Swirl

To further understand the effect of swirl on the streamwise development of momentumless wakes, Fig. 10 compares measurements in the two momentumless wakes without[2] and with swirl, with respect to a few key parameters. From the centerline and minimum

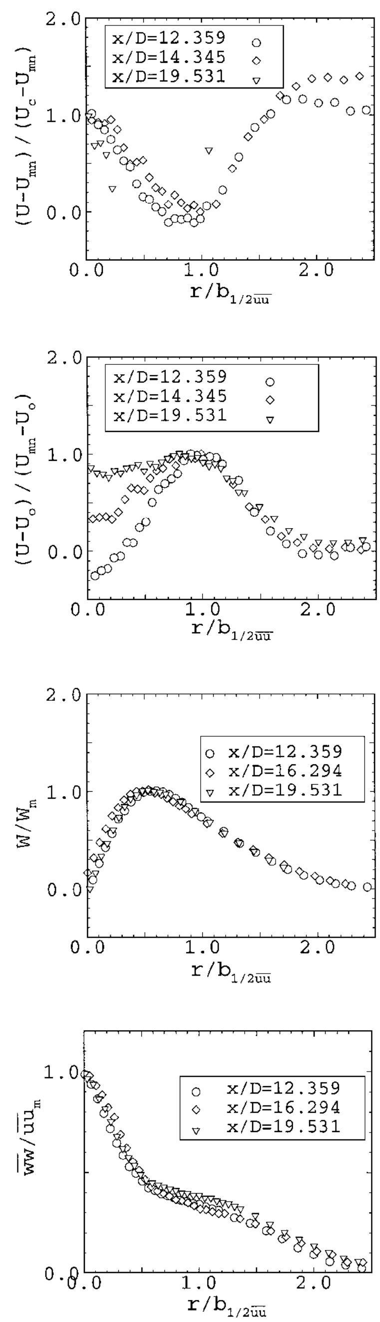

Fig. 9 Similarity of velocity and turbulence profiles.

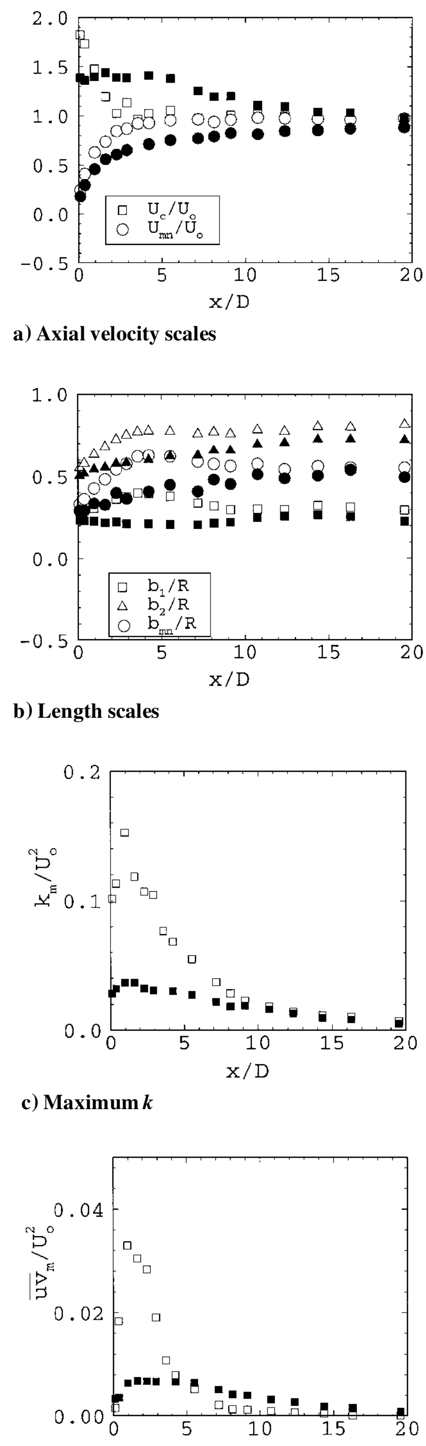

a) Axial velocity scales

b) Length scales

c) Maximum *k*

d) Maximum *uv*

Fig. 10 Momentumless wakes with and without swirl characteristic scales: momentumless swirling wake (open symbols) and momentumless wake (filled symbols).

axial velocities shown in Fig. 10a, it is clear that swirl induces a rapid decrease of mean shear. The two velocity scales approach the freestream velocity within a streamwise distance of $x/D = 6$ in the presence of swirl, whereas a comparable condition is barely achieved by the last measurement station in the absence of swirl ($x/D \sim 20$). The diminution of mean shear is, of course, associated with decreasing turbulence production. The three length scales of the axial velocity profile, namely, b_1, b_{mn}, and b_2 (see Fig. 2) are compared in Fig. 10b. It is clear that all are larger in the presence of swirl, as already noted from the profiles in the preceding section. However, the present comparison shows that b_1, which is a measure of the inner region, and b_{mn}, which may be regarded as the boundary between the inner and outer regions, both indicate significant influence of swirl, particularly in the intermediate region. On the other hand, the length b_2, characterizing the outer layer, originating from the body boundary layer, develops without much evidence of swirl effects.

The decrease in turbulence production is apparent from the development of the maximum values of the turbulence kinetic energy (Fig. 10c) and shear stresses (Fig. 10d). Although the swirling wake initially contains much larger turbulence energy, the levels in the two cases are almost identical beyond $x/D = 12 \sim 13$, the end of the intermediate region. Even more significantly, the shear stress in the swirling wake practically vanishes by the same distance. This supports the suggestion made in prior studies[8,9] that the flow resembles decaying homogeneous turbulence. Clearly, this situation is reached much earlier in the presence of swirl.

VI. Propeller-Driven Flow vs Swirling Jet-Driven Flow

The most obvious difference between these two flows is the absence, in the case of the wake of the swirling jet-driven body, of

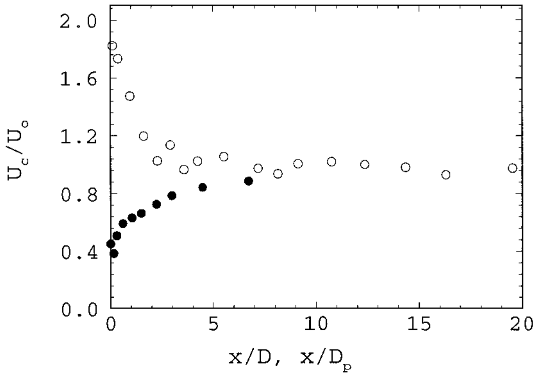

a) Comparisons of U_c

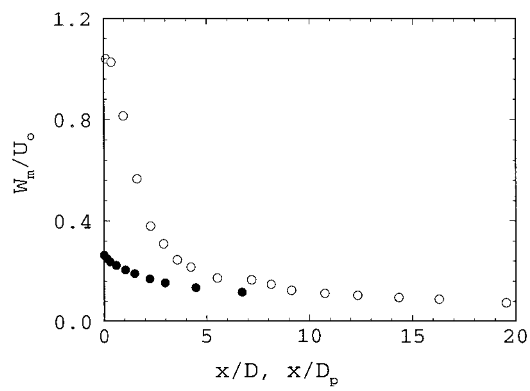

b) Comparisons of W_m

Fig. 11 Comparisons of axial and tangential velocity scales: swirling jet-driven flow (open symbols) and propeller-driven flow (filled symbols).

flow periodicity resulting from a finite number of propeller blades. In a reference frame fixed to the body, the flow in the wake of the propeller is periodic in time and requires phase-averaging techniques to distinguish the blade wakes from the wake of the body. However, measurements behind propellers[3–5,10] show that the periodicity is practically nonexistent (i.e., the blade wake is smeared into the background flow) within approximately two propeller diameters. Therefore, it is meaningful to make at least qualitative comparisons with previous data from wakes of propeller-driven bodies. In fact, quantitative comparisons with the data of Hyun and Patel,[3,4] who employed a three-blade propeller of diameter $D_p = 10.13$ cm, are also possible because the present study employed essentially the same body and experimental conditions.

The streamwise variation of the centerline axial velocity, using the jet, D, and propeller, D_p, diameters, as appropriate, to nondimensionalize the streamwise distance, is presented in Fig. 11a, along with the data of Hyun and Patel.[3,4] The results should be interpreted taking into account that immediately downstream of a propeller the maximum axial velocity occurs some distance away from the centerline (around $r/R_p = 0.7$ in Refs. 3 and 4), depending on the propeller characteristics. It is significant that the freestream velocity is approached in the three data sets within about seven diameters in spite of the grossly different initial conditions. Figure 11b presents the evolution of the maximum swirl velocity. It is found that the propeller-induced swirl is considerably smaller than in the jet, in spite of the matched tangential momentum and that it decays faster.

The similarities and differences in the turbulence in the two cases are shown by the streamwise development of the maximum values of the turbulence kinetic energy and two of the shear stresses in Figs. 12a and 12b. The turbulence in the near field is much larger for the swirling jet-driven body. However, the shear stresses become negligible in all cases by about 10 diameters, although differences persist in the turbulence kinetic energy. The two flows, therefore, approach the condition of vanishing mean shear and negligible turbulence production within 10 jet/propeller diameters.

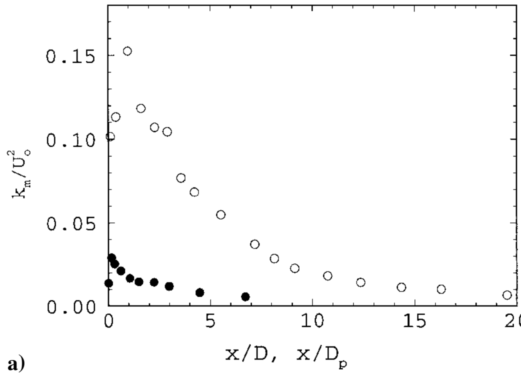

a)

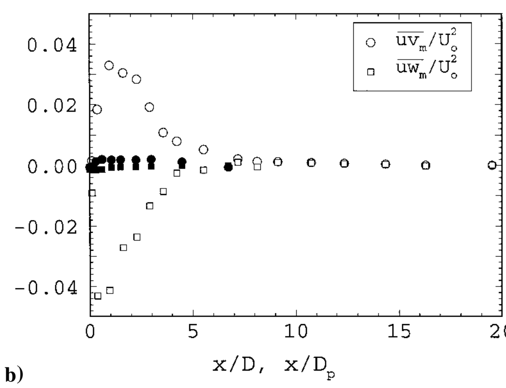

b)

Fig. 12 Comparisons of turbulence kinetic energy and shear stresses: swirling jet-driven flow (open symbols) and propeller-driven flow (filled symbols).

VII. Conclusions

Detailed mean-flow and turbulence measurements in the momentumless wake of the axisymmetric body propelled by a swirling jet are reported. The data elucidate the process of mixing between the boundary layer of the body and the jet, and the evolution of the momentumless wake. The main findings can be summarized as follows:

1) The wake evolves in at least three stages. The first of these is the near wake, extending to about 3 jet diameters, where the flow from the near-wall region of the boundary layer mixes with the jet periphery to produce an intense shear layer, distinct from the swirl-induced shear layer that is present at the jet center. There is rapid decay of the mean shear and turbulence in this region. In the second, intermediate region, extending to about 13 jet diameters, the mixing penetrates to the wake centerline, the individual shear layers are assimilated, the pressure field induced by the body geometry and the swirling jet decays, and the mean shear and the Reynolds shear stresses become negligible by the end of this region. In the third region, called the developed wake, the flow acquires some of the characteristics of a single shear layer, with very low levels of mean shear and shear stresses, implying negligible production of new turbulence and decay of the normal stresses produced upstream.

2) Analysis of the data in the format of classical similarity theory reveals that the axial and swirling flows develop at quite different rates, as do the corresponding turbulence characteristics. The swirl decays at a slower rate than the axial velocity excess, maintains a remarkable coherence along the flow, and shows agreement with predictions of similarity theory. Properties of the axial flow do not show agreement with similarity analysis. The axial velocity and turbulence profiles indicate that two different scales are needed to represent the inner and outer regions, as in the case of the momentumless wake without swirl.[6]

3) Swirl is associated with a rapid decrease of mean shear and turbulent shear stress, which means lower production of turbulence in comparison to the momentumless wake without swirl.[6] Almost identical levels of turbulence are found for both momentumless wakes after approximately 12 jet diameters.

4) The momentumless wake generated by the swirling jet was compared to that generated by a propeller.[3,4] The near fields of the

two flows are grossly different, but strong similarity of both mean flows is found after 7 diameters and at around 10 diameters the production of turbulence is negligible.

References

[1]Sirviente, A. I., and Patel, V. C., "Experiments in the Turbulent Near Wake of an Axisymmetric Body," *AIAA Journal*, Vol. 37, No. 12, 1999, pp. 1670–1673.

[2]Sirviente, A. I., and Patel, V. C., "Wake of a Self-Propelled Body, Part 1: Momentumless Wake," *AIAA Journal*, Vol. 38, No. 4, 2000, pp. 613–619.

[3]Hyun, B. S., and Patel, V. C., "Measurements in the Flow Around a Marine Propeller at the Stern of an Axisymmetric Body. Part I. Circumferentially-Averaged Flow," *Experiments in Fluids*, Vol. 11, No. 1, 1991, pp. 33–44.

[4]Hyun, B. S., and Patel, V. C., "Measurements in the Flow Around a Marine Propeller at the Stern of an Axisymmetric Body. Part II. Phase-Averaged Flow," *Experiments in Fluids*, Vol. 11, No. 2, 1991, pp. 105–117.

[5]Faure, T., and Robert, G., "Turbulent Kinetic Energy Balance in the Wake of a Self-Propelled Body," *Experiments in Fluids*, Vol. 21, No. 4, 1996, pp. 268–274.

[6]Sirviente, A. I., "Wake of an Axisymmetric Body Propelled by a Jet with and Without Swirl," Ph.D. Dissertation, Dept. of Mechanical Engineering, Univ. of Iowa, Iowa City, IA, 1996.

[7]Ferry, M., and Piquet, J., "Sillage Visqueux Lointain d'un Corps Sous-Marin Autopropulse," SIREHNA, Rapport d'Etude 86/14/R, Nantes, France, 1987.

[8]Ridjanovic, M., "Wake with Zero Change of Momentum Flux," Ph.D. Dissertation, Dept. of Mechanical Engineering, Univ. of Iowa, Iowa City, IA, 1963.

[9]Wang, H., "Flow Behind a Point Source of Turbulence," Ph.D. Dissertation, Dept. of Mechanical Engineering, Univ. of Iowa, Iowa City, IA, 1965.

[10]Petersson, P., Larson, M., and Jonsson, L., "Measurements of the Velocity Field Downstream an Impeller," *Journal of Fluids Engineering*, Vol. 118, No. 3, 1996, pp. 602–610.

F. W. Chambers
Associate Editor